Journal of Zhejiang University SCIENCE A
ISSN 1673-565X (Print); ISSN 1862-1775 (Online)
www.zju.edu.cn/jzus; www.springerlink.com
E-mail: jzus@zju.edu.cn

Zero-voltage switching converter absorbing parasitic parameters for super high frequency induction heating

Zheng-shi WANG†, Hui-ming CHEN

(*School of Electrical Engineering, Zhejiang University, Hangzhou 310027, China*)

†E-mail: wzs@zju.edu.cn

Received Apr. 3, 2007; revision accepted Dec. 24, 2007; published online Mar. 6, 2008

Abstract: This paper presents a novel mega-Hz-level super high frequency zero-voltage soft-switching converter for induction heating power supplies. The prominent advantage of this topology is that it can absorb both inductive and capacitive parasitic components in the converter. The switch devices operate in a zero-voltage soft-switching mode. Consequently, the high voltage and high current spikes caused by parasitic inductors or capacitors oscillation do not occur in this circuit, and the high power loss caused by high frequency switching can be greatly reduced. A large value inductor is adopted between the input capacitor and the switches, thus, this novel converter shares the benefits of both voltage-type and current-type circuits simultaneously, and there are no needs of dead time between two switches. The working principles in different modes are introduced. Results of simulation and experiments operated at around 1 MHz frequency verify the validity of parasitic components absorption and show that this converter is competent for super high frequency applications.

Key words: Induction heating, Super high frequency, Soft-switching converter, Parasitic parameters
doi:10.1631/jzus.A071177 **Document code:** A **CLC number:** TM92

INTRODUCTION

Mega-Hz-level super high frequency induction heating is provided with particular advantages in the application of metal surface treatment. However, power oscillators with radio tubes still predominate these areas because of the frequency consideration. The fact is that the apparatus built on radio tubes has many serious drawbacks, such as low efficiency (50% in normal), short life, and warm-up request. Solid-state induction heating power supplies, with fast power electronic switching devices, such as MOSFET and IGBT, will greatly improve the performances of these apparatus, especially the power efficiency. Many achievements have been made in low power apparatus (Czarkowski and Kazmierczuk, 1998; Wang *et al*., 1998; Espi *et al*., 2000; Yoshida *et al*., 2001; Moisseev *et al*., 2003; Chang *et al*., 2004; Mollov *et al*., 2004). Comparing with low frequency circuits, super high frequency converters have to solve some special problems in circuit design and producing craft (Calleja and Ordonez, 1999; Dede *et al*., 1999; Theodoridis and Mollo, 2004). The first is the inductive and capacitive parasitic parameters in devices and circuit wires or routes. The equivalent impedance of these inductive and capacitive parasitic parameters cannot be neglected, otherwise they will cause severe oscillations, as well as the voltage and current spikes which may damage the switching devices (Chen *et al*., 2001). The second is the huge power loss caused by high frequency switching. It is the reason that super high frequency converters should have the abilities to absorb these parasitic components and thus minimize the switching loss. Both class-D and class-E circuits are quite good topologies in high frequency applications (Czarkowski and Kazmierczuk, 1998; Hinchliffe and Hobson, 1998; Chang *et al*., 2004; Lee and Hyun, 2004) and have been widely used in RF areas. But they are not suitable for induction heating applications because the load varies seriously when the metal piece is heated.

In this paper, a novel dual-LLC resonant tank soft-switching converter is proposed, in which both inductive and capacitive parasitic components in circuit and devices can be absorbed while all MOSFET devices operate in the zero-voltage soft-switching mode. Moreover, this topology has two more advantages. A large value inductor is inset between the input bank capacitor and the switches, so this converter may share the benefit of current-type circuit, and the dead time between the two switches are unnecessary. In the load tank, a series inductor is used as part of the compensator, which greatly improves the load short circuit abilities. The operating principle of the converter is introduced in detail, and the key waveforms in resonant tanks are analyzed. Results of simulation and experiments operated at around 1 MHz are given.

PRINCIPLE OF THE CONVERTER

The proposed novel converter is shown in Fig.1. Compared with a normal "H-bridge" type converter, two inductors L_{a1} and L_{a2} are employed to replace the upside switches. There are two LLC tanks in this converter. One is called "load LLC tank", which is made up of L_s, C, L_p and R_e (L_p and R_e are equivalent inductor and resistor of the induction wire and load, respectively). Another is called "auxiliary resonant tank", including L_a (L_{a1} or L_{a2}), C_a (C_{a1} or C_{a2}), and load equivalent impedance Z_L. It is the auxiliary LLC resonant tank that helps Q_1 and Q_2 work in zero-voltage soft-switching mode. Inductors L_{a1}, L_{a2} and L_s can absorb the parasitic inductive components of the circuit, and C_{a1}, C_{a2} can absorb the parasitic capacitors in the switch devices. All these parasitic components are used as elements in the resonant loop. So, parasitic oscillations and high voltage/current surges caused by these parasitic components can be effectively eliminated. The dead time between Q_1 and Q_2, which is quite common in the voltage-type converter, is not needed because the inductor L_d is set between the input and the switches. Therefore, this topology is competent to work at super high frequency. Other benefits of this topology include that this series-connected inductor (i.e., L_s in the load tank) can improve the load short-circuit protection abilities of the converter and has the same function as that of a normal matching transformer.

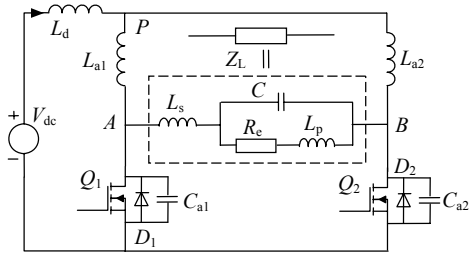

Fig.1 Super high frequency zero-voltage switching converter for induction heating

Impedance characteristic of load LLC tank

The load LLC tank is made up of induction coil (equivalent inductor L_p and equivalent resistance R_e), parallel compensator capacitor C, and series compensator inductor L_s. This series and parallel compensator can improve not only the power factor of the load loop, but also the load short-circuit ability. Moreover, this configuration has the same function as the normal transformer to transform the voltage value. Thus, the output transformer used for load matching can be omitted. Consequently, the power efficiency will be improved, and the weight and size of the power supply can be reduced. The impedance characteristic of load LLC tank plays an important role in the converter operation and power delivery. The impedance of load LLC tank Z_L can be expressed as

$$\begin{aligned} Z_L &= \mathrm{j}\omega L_s + \frac{1}{\mathrm{j}\omega C + \dfrac{1}{R + \mathrm{j}\omega L_p}} \\ &= \frac{(R - RL_sC\omega^2) + \mathrm{j}(L_s\omega + L_p\omega - L_pL_s\omega^3)}{1 - L_pC\omega^2 + \mathrm{j}RC\omega}. \end{aligned} \tag{1}$$

The magnitude and phase are

$$\begin{cases} |Z_L| = \dfrac{\sqrt{(R - RL_sC\omega^2)^2 + (L_s\omega + L_p\omega - L_pL_s\omega^3)^2}}{\sqrt{(1 - L_pC\omega^2)^2 + (RC\omega)^2}}, \\ \varphi = \arctan\left(\dfrac{L_s\omega + L_p\omega - L_pL_s\omega^3}{R - RL_sC\omega^2}\right) - \arctan\left(\dfrac{RC\omega}{1 - L_pC\omega^2}\right). \end{cases} \tag{2}$$

Fig.2 shows the load LLC tank magnitude and phase with different frequencies. There are two resonant poles in the load LLC tank: the series pole ω_o and the parallel resonant pole ω_p:

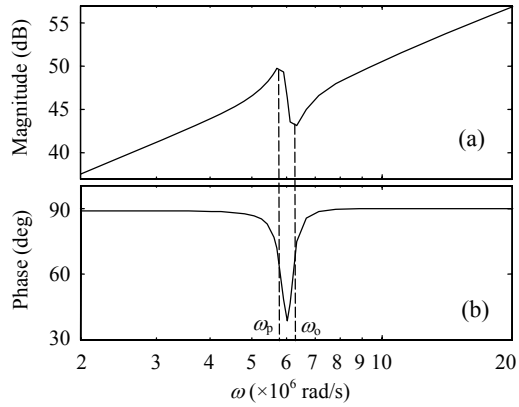

Fig.2 Magnitude (a) and phase (b) of the load LLC tank

$$\omega_o = 1\Big/\sqrt{\frac{L_p L_s}{L_p + L_s}C}, \quad \omega_p = 1\Big/\sqrt{L_p C}.$$

In order to reduce the reactive power delivery between the load and the power supply and get the maximum output power in the load, the switching frequency of the converter is set at series pole ω_o. If the output power should be regulated, one can choose $\omega \geq \omega_o$. The maximum output at ω_o can be expressed as

$$P_{max} \approx \frac{u_{AB}^2}{R}\left(\frac{L_p}{L_s}\right)^2. \tag{3}$$

Eq.(3) shows that the inductors L_p and L_s have the voltage transformation function, just like the general voltage transformer.

Analysis of the auxiliary resonant LLC tank

There is another LLC tank in the proposed converter, called "auxiliary resonant LLC tank", including L_a, C_a and Z_L. Fig.3a shows the circuit when Q_1 is off and Q_2 is on. Fig.3b is the equivalent circuit of Fig.3a, where

$$\begin{cases} R'_e = [R_e^2 + (\omega L_e)^2]/R_e, \\ C'_{a1} = C_{a1} - L_e/[(\omega L_e)^2 + R_e^2]. \end{cases} \tag{4}$$

There is a similar equivalent circuit when Q_1 is on and Q_2 is off. Based on the topology and symmetry of the converter, one can get

$$u_{AB} = u_{Q_1} - u_{Q_2}, \tag{5}$$

$$u_P = \left(u_{Q_1} + u_{Q_2}\right)\Big/2. \tag{6}$$

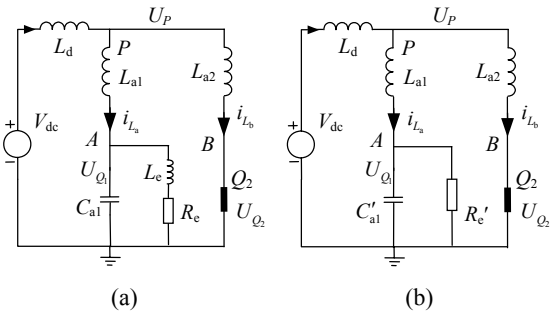

Fig.3 Auxiliary resonant circuits in case of Q_2
(a) Steady circuit; (b) Equivalent circuit

In the auxiliary resonant tank, the voltage and current are governed by

$$\begin{cases} L_a \dfrac{di_{L_a}}{dt} + u_Q(t) = u_P, \quad i_{L_a} = \dfrac{u_Q}{R'_e} + C'_a \dfrac{du_Q}{dt}, \\ u_P = u_Q/2, \quad L_b \dfrac{di_{L_b}}{dt} = u_P. \end{cases} \tag{7}$$

One can get

$$\frac{d^2u_Q(t)}{dt^2} + \frac{1}{R'_e C'_a}\frac{du_Q(t)}{dt} + \frac{1}{2L_a C'_a}u_Q(t) = 0. \tag{8}$$

When $R'_e > \sqrt{L_a/(2C_a)}$, the solution of this second-order differential equation can be expressed as

$$u_Q(t) = U_{AM} e^{\sigma t} \sin(\omega_d t + \varphi), \tag{9}$$

where

$$\sigma = -1/(2R'_e C'_a), \quad \omega_d = \frac{1}{2}\sqrt{(R'_e C'_a)^{-2} - 2/(L_a C'_a)},$$

U_{AM} is the magnitude with the initial value being

$$u_Q(0) = 0, \quad \frac{du_Q(0)}{dt} = \frac{i_{L_{a1}}(0)}{C'}.$$

There are three kinds of frequency in this converter: the switching frequency f_s of the converter, the load LLC inherent resonant frequency f_L, and the auxiliary inherent resonant tank frequency f_d. In most induction heating applications, phase lock loop (PLL) is often implemented to keep f_s=f_L. Moreover, in order to let Q_1 and Q_2 operate in zero-voltage soft-switching mode, these frequencies should be

$$f_s = f_L < f_d. \tag{9}$$

D is defined as $D=f_s/f_d<1$. Obviously, as $f_s<f_d$, there is an interval when the body diode of the MOSFET turns on, and at that time, $u_Q(t)$ is zero. Thus, in half a cycle, the waveform of $u_Q(t)$ has two parts: the resonant trail governed by Eq.(8) and the zero-voltage trail.

Because the average voltage across the inductor is zero in steady state, one can get

$$V_{dc} = \frac{1}{2\pi}\int_0^{2\pi}(u_{L_d} + u_P)\mathrm{d}(\omega t) = 0 + \frac{1}{2\pi}\int_0^{2\pi} u_P \mathrm{d}(\omega t). \tag{10}$$

If the value of $\sigma=-(R_e'C_a')^{-1}$ is not so large, the magnitude of $u_Q(t)$ is

$$U_{AM} = \frac{\pi}{2D}V_{dc}. \tag{11}$$

Thus, in one cycle, the voltages of $u_{Q_1}(t)$, $u_{Q_2}(t)$, $u_P(t)$ and $u_{AB}(t)$ can be expressed as

$$U_{Q_1}(t) = \begin{cases} 0, & 0 < \omega_d t \le (3-D)\pi/2, \\ & \text{or } (3+D)\pi/2 < \omega_d t \le 2\pi; \\ \dfrac{\pi V_{dc}}{D} e^{\sigma t} \sin\left[\dfrac{\omega_d t - (3-D)\pi/2}{D}\right], & \\ & (3-D)\pi/2 < \omega_d t < (3+D)\pi/2. \end{cases} \tag{12}$$

$$U_{Q_2}(t) = \begin{cases} 0, & 0 < \omega_d t \le (1-D)\pi/2, \\ & \text{or } (1+D)\pi/2 < \omega_d t \le 2\pi; \\ \dfrac{\pi V_{dc}}{D} e^{\sigma t} \sin\left[\dfrac{\omega_d t - (1-D)\pi/2}{D}\right], & \\ & (1-D)\pi/2 < \omega_d t < (1+D)\pi/2. \end{cases} \tag{13}$$

$$U_P(t) = \begin{cases} 0, & 0 < \omega_d t \le (1-D)\pi/2, \\ & \text{or } (1+D)\pi/2 < \omega_d t \le (3-D)\pi/2, \\ & \text{or } (3+D)\pi/2 < \omega_d t \le 2\pi; \\ \dfrac{\pi V_{dc}}{2D} e^{\sigma t} \sin\left[\dfrac{\omega_d t - (1-D)\pi/2}{D}\right], & \\ & (1-D)\pi/2 < \omega_d t < (1+D)\pi/2; \\ \dfrac{\pi V_{dc}}{2D} e^{\sigma t} \sin\left[\dfrac{\omega_d t - (3-D)\pi/2}{D}\right], & \\ & (3-D)\pi/2 < \omega_d t < (3+D)\pi/2. \end{cases} \tag{14}$$

$$U_{AB}(t) = \begin{cases} 0, & 0 < \omega_d t \le (1-D)\pi/2, \\ & \text{or } (1+D)\pi/2 < \omega_d t \le (3-D)\pi/2, \\ & \text{or } (3+D)\pi/2 < \omega_d t \le 2\pi; \\ \dfrac{-\pi V_{dc}}{D} e^{\sigma t} \sin\left[\dfrac{\omega_d t - (1-D)\pi/2}{D}\right], & \\ & (1-D)\pi/2 < \omega_d t < (1+D)\pi/2; \\ \dfrac{\pi V_{dc}}{D} e^{\sigma t} \sin\left[\dfrac{\omega_d t - (3-D)\pi/2}{D}\right], & \\ & (3-D)\pi/2 < \omega_d t < (3+D)\pi/2. \end{cases} \tag{15}$$

Fig.4 shows the voltage waveforms of U_{Q_a}, U_{AB}, U_P with control signals of Q_1 and Q_2.

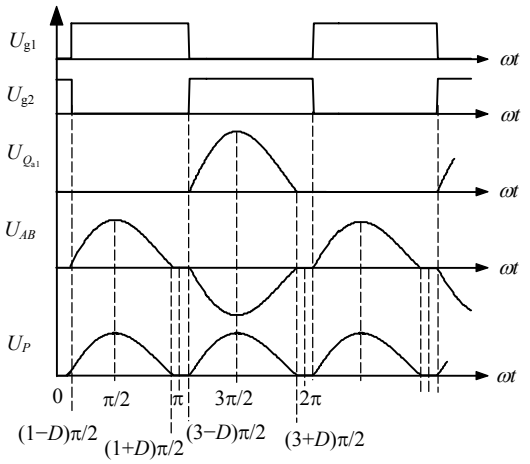

Fig.4 Voltage waveforms of U_g, $U_{Q_{a1}}$, U_{AB} and U_P

Operation modes of the converter

In the proposed converter, there are six working modes in one operation cycle.

Mode 1 [t_1~t_2]: Q_1 turns on at this time, however, the current flows through the body diode D_1. So, Q_1 turns on in zero-voltage condition. When $t=t_1$, Q_2 turns off. Because a large capacitor C_{a2} is paralleled with Q_2, the voltage across Q_2 rises slowly, so the switching losses of Q_1 and Q_2 will be quite small.

Mode 2 [t_2~t_3]: at t_2, the current flowing through D_1 decreases to zero and starts to flow into Q_1.

Mode 3 [t_3~t_4]: at t_3, U_{Q_2} decreases to zero, and D_2 starts to turn on. U_{Q_2} is clamped at zero, and the auxiliary resonant stops.

Mode 4 [t_4~t_5]: Q_1 is turned off at t_4, the current switches to C_a, and a new auxiliary resonant in C_{a1}',

R'_e and L_{a1} starts to work, U_{Q_1} rises as governed by Eq.(8).

Mode 5 [t_5~t_6]: at t_5, the current flowing through D_2 decreases to zero, and starts switching to Q_2.

Mode 6 [t_6~t_7]: at t_6, U_{Q_1} decreases to zero, and D_1 starts to turn on. U_{Q_1} is clamped to zero, and the auxiliary resonant stops working.

Fig.5 shows the equivalent circuits of the six operation modes. Fig.6 shows the key waveforms in the converter during one operation cycle. U_{g1}/U_{g2} are gate signals of Q_1/Q_2, U_{Q_1}/U_{Q_2} are voltages across the switches, U_{AB} and U_C are voltages across points A, B and capacitor C, respectively. i_{Q_1}, i_{Q_2}, i_{D_1}, i_{D_2}, i_{C_1}, i_{C_2} are the currents flowing through the devices of Q_1, Q_2, D_1, D_2, C_1, C_2, respectively.

Power regulation

In most cases, the output power should be variable. In this converter, two different approaches can be adopted for power regulation. One simple way is to change the input DC voltage V_{dc}, and the output power will be changed with changed V_{dc}. However, in order to regulate the input DC voltage, an extra DC/DC converter is required. Inevitably, the total efficiency of power conversion will be greatly reduced, and the cost will be increased. Another method to regulate the output power is to change the switching frequency of the converter. This method is based on the impedance characteristic of the load LLC tank. Consequently, the PPL technique cannot be used in this power regulation method.

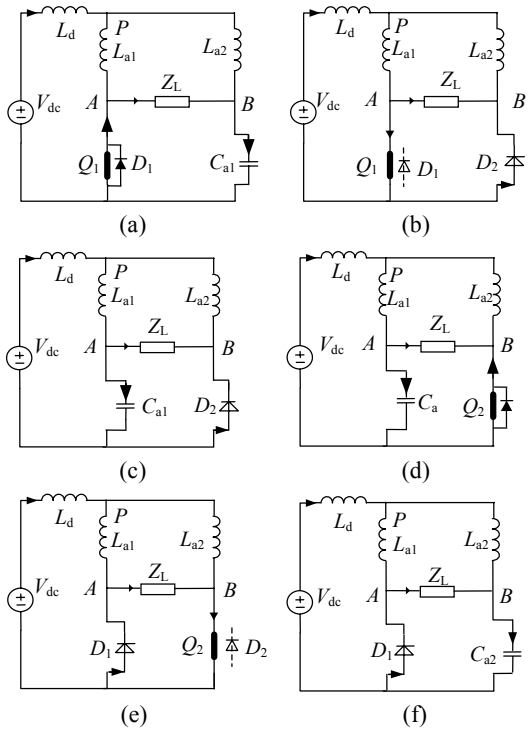

Fig.5 Equivalent circuits of the six operation modes
(a) Mode 1 [t_1~t_2]; (b) Mode 2 [t_2~t_3]; (c) Mode 3 [t_3~t_4]; (d) Mode 4 [t_4~t_5]; (e) Mode 5 [t_5~t_6]; (f) Mode 6 [t_6~t_7]

SIMULATION AND EXPERIMENTAL RESULTS

The parameters of the converter in simulation are: V_{dc}=150 V, L_d=200 μH, C_{a1}=C_{a2}=2.5 nF, L_{a1}=L_{a2}= 5 μH, L_s=35 μH, L_p=2.4 μH, C=12 nF, the switching frequency f_s is around 1.0 MHz. Fig.7 shows the simulation results. Obviously, Q_1 turns on in ZVS mode, and turns off with very low dV/dt rising ratio. Since the parasitic parameters are absorbed by the circuit components L_a, L_s and C_a, the voltage and current traces are all quite clear.

Fig.8 gives the experimental waveforms of U_{Q_1} and U_P when V_{dc} is 54 V. The relationship between the magnitudes of U_{Q_1} and U_P (i.e., $U_{Q_1AM} = 2U_{PAM}$) verifies the validity of the theoretical analysis aforementioned.

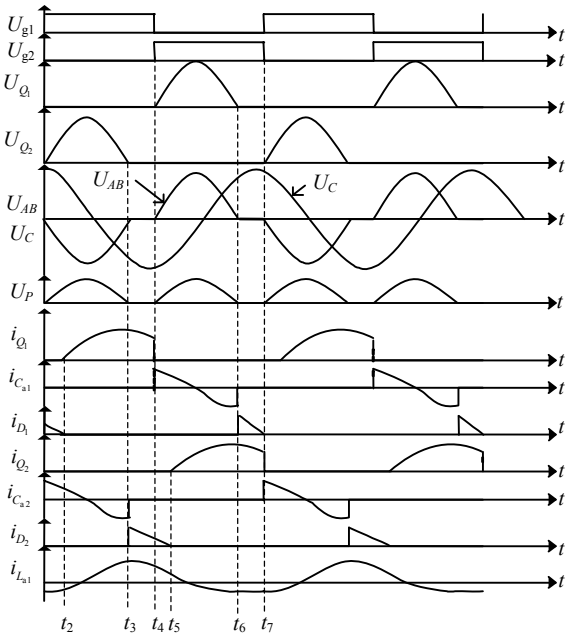

Fig.6 Key waveforms in the converter during one operation cycle

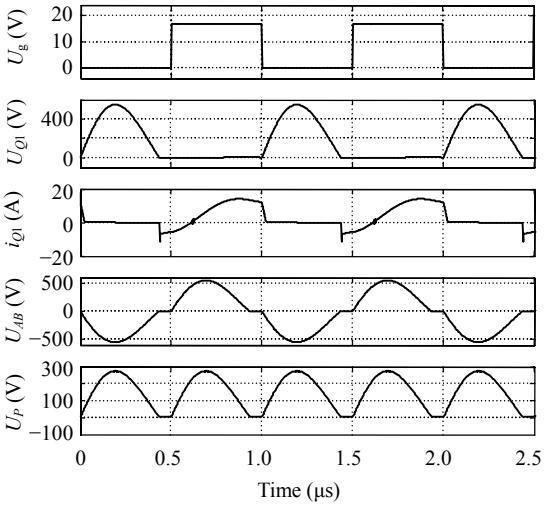

Fig.7 Simulation results of U_{Q1}, i_{Q1}, U_{AB} and U_P

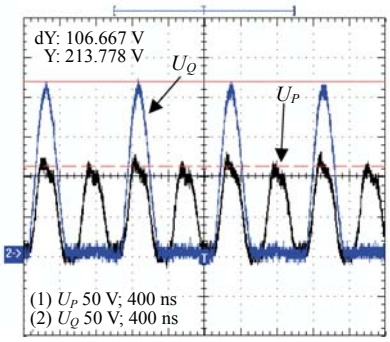

Fig.8 Experimental waveforms of the switch and point *P*

One method to regulate the output power is to change f_s. Fig.9 shows the U_{AB} and U_C waveforms in different switching frequencies of 973 kHz, 1.008 MHz and 1.049 MHz when the PPL is removed. As the inherent resonant frequency f_L of the load LLC tank is away from f_s, the voltage across the load U_C decreases.

Obviously, when f_s is changed, the current, voltage, output power, and the converter efficiency would change greatly. Table 1 shows these trends with different f_s, where $i_{Ls\text{-}p}$ is the peak current of the series inductor L_s, $i_{Lp\text{-}p}$ is the peak current of the parallel inductor L_p, $U_{Q\text{-}p}$ is the peak voltage of the switch Q, and P_o is the output power. These data are measured when V_{dc} is 200 V.

Fig.10 shows the converter efficiency η with different f_s. In order to obtain high conversion efficiency and maximum output power, f_s should be close to the inherent pole frequency of the LLC tank.

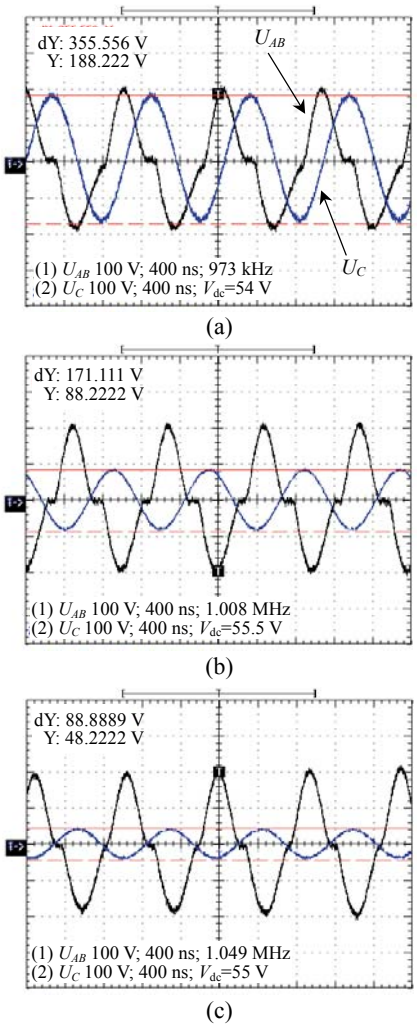

Fig.9 Experimental waveforms of U_C and U_{AB}
(a) f_s=973 kHz; (b) f_s=1.008 MHz; (c) f_s=1.049 MHz

Table 1 Voltage, current, and output power with different switching frequencies*

f_s (kHz)	$i_{Ls\text{-}p}$ (A)	$i_{Lp\text{-}p}$ (A)	$U_{Q\text{-}p}$ (V)	P_o (W)
860	2.3	15.7	805	123.8
880	2.4	18.2	785	165.7
900	2.3	21.9	762	239.9
920	2.4	27.4	736	375.5
940	2.5	35.4	715	626.8
960	7.8	45.0	720	1015.1
980	5.0	43.3	750	937.7
1000	5.0	31.7	750	502.6
1020	4.5	22.3	732	248.7
1040	4.0	16.8	715	140.7
1060	3.7	13.0	700	84.9

* Data measured when V_{dc}=200 V. f_s: switching frequency; $i_{Ls\text{-}p}$, $i_{Lp\text{-}p}$: peak currents of the series inductor L_s and the parallel inductor L_p, respectively; $U_{Q\text{-}p}$: peak voltage of the switch Q; P_o: output power

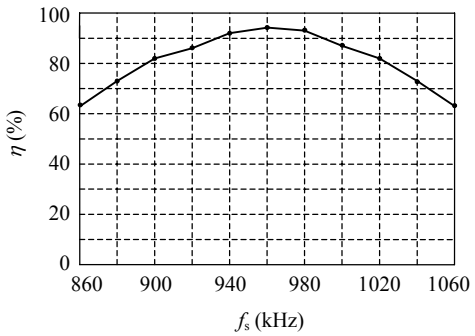

Fig.10 Relationship of the power conversion efficiency and the switch frequency

Fig.11 shows the different load voltages U_C with different compensation inductors L_s. U_C increases from 128 V to 232 V when L_s reduces from 35 μH to 26 μH. From this view, L_s has the function of normal voltage transformation.

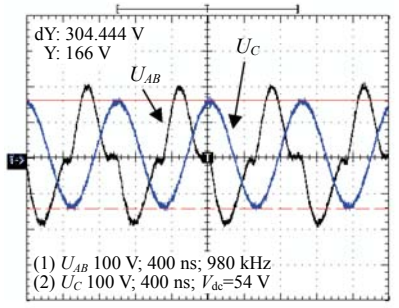

(a)

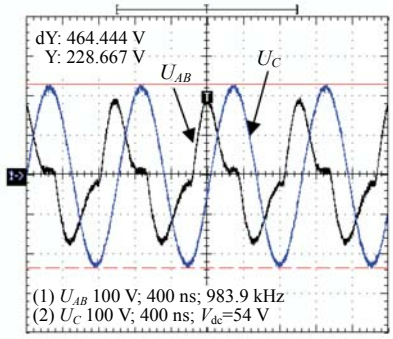

(b)

Fig.11 Waveforms of U_C and U_{AB} in different L_s
(a) L_s=35 μH; (b) L_s=26 μH

CONCLUSION

A novel zero-voltage soft-switching converter with dual-LLC resonant tank, which can absorb the parasitic components in the circuit and devices, is proposed for super high frequency induction heating power supplies. Most inductive and capacitive parasitic parameters can be used as elements of the resonant tank. Reasonable switching frequency can be selected according to the circuit parameters and the needs of application. Thus, high voltage and current spikes will not appear, and the switching loss can be greatly reduced. Key waveforms in the converter from simulation and experiments operated at around 1 MHz are given. The smooth voltage and current waveforms verify the validity of parasitic components absorption, and the mega-Hz frequency operation verifies that this converter is competent for super high frequency applications.

References

Calleja, H., Ordonez, R., 1999. Improved Induction Heating with Power Factor Correction. Proc. IEEE Power Electronics Specialists Conf., p.1132-1137.

Chang, J.S., Tan, M.T., Cheng, Z., Tong, Y.C., 2004. Analysis and design of power efficient class D amplifier output stages. *IEEE Trans. on Circuits & Syst. I-Fundam. Theory & Appl.*, **47**(6):897-902. [doi:10.1109/81.852942]

Chen, M.P., Chen, J.K., Murata, K., Nakahara, M., Harada, K., 2001. Surge analysis of induction heating power supply with PLL. *IEEE Trans. on Power Electr.*, **16**(5):702-709. [doi:10.1109/63.949503]

Czarkowski, D., Kazmierczuk, M.K., 1998. ZVS class D series resonant inverter-discrete-time state-space simulation and experimental results. *IEEE Trans. on Circuits & Syst. I-Fundam. Theory & Appl.*, **45**(11):1141-1147. [doi:10.1109/81.735436]

Dede, E.J., Jordan, J., Esteve, V., Espi, J.M., Casans, S., 1999. Series and Parallel Resonant Inverters for Induction Heating Under Short-Circuit Conditions Considering Parasitic Components. Proc. Power Electronics and Device Systems, p.659-662.

Espi, J.M., Navarro, A.E., Maicas, J., Ejea, J., Casans, S., 2000. Control Circuit Design of the L-LC Resonant Inverter for Induction Heating. Proc. IEEE Power Electronics Specialists Conf., p.1430-1435.

Hinchliffe, S., Hobson, L., 1998. High power class-E amplifier for high-frequency induction heating applications. *IEE Proc.-Electr. Power Appl.*, **24**(14):886-888.

Lee, D., Hyun, D., 2004. Hybrid control scheme of active-clamped class E inverter with induction heating power applications. *IEE Proc.-Electr. Power Appl.*, **151**(6):704-710. [doi:10.1049/ip-epa:20040582]

Moisseev, S., Muraoka, H., Nakamura, M., Okuno, A., Hiraki, E., Nakaoka, M., 2003. Zero voltage soft switching PWM high-frequency inverter using IGBTs for induction heated fixed roller. *IEE Proc.-Electr. Power Appl.*, **150**(2):237-244. [doi:10.1049/ip-epa:20030120]

Mollov, S.V., Theodoris, M., Forsyth, A.J., 2004. High frequency voltage-fed inverter with phase-shift control for induction heating. *IEE Proc.-Electr. Power Appl.*, **151**(1): 12-18. [doi:10.1049/ip-epa:20031058]

Theodoridis, M.P., Mollo, S.V., 2004. Improved Gate Driver for a 13.56 MHz Resonant Inverter. Proc. 2nd IEE Int. Conf. on Power Electronics, Machines and Drives, **1**:143-148.

Wang, S., Izaki, K., Hirota, I., Yamashita, H., 1998. Induction-heating cooking appliance using new quasi-resonant ZVS-PWM inverter with power factor correction. *IEEE Trans. on Ind. Appl.*, **34**(4):705-712. [doi:10.1109/28.703961]

Yoshida, D., Kifune, H., Hatanaka, Y., 2001. ZCS High Frequency Inverter for Induction Heating with Quasi-constant Frequency Power Control. Proc. 4th IEEE Int. Conf. on Power Electronics and Drive Systems, **2**:755-759. [doi:10.1109/PEDS.2001.975413]